Effect of shell structure in the fusion reactions ^{82}Se+^{134}Ba and ^{82}Se+^{138}Ba

K. Satou,[1,2] H. Ikezoe,[1] S. Mitsuoka,[1] K. Nishio,[1] and S. C. Jeong[3]
[1]*Advanced Science Research Center, Japan Atomic Energy Research Institute, Tokai-mura, Ibaraki 319-1195, Japan*
[2]*Institute of Physics and Tandem Accelerator Center, University of Tsukuba, Tsukuba-shi, Ibaraki 305-8577, Japan*
[3]*Institute of Particle and Nuclear Studies, KEK, Tsukuba-shi, Ibaraki 305-0801, Japan*
(Received 31 October 2001; published 18 April 2002)

The dependence of fusion on the nuclear shell structure was investigated for the two reaction systems ^{82}Se+^{138}Ba and ^{82}Se+^{134}Ba, where the nucleus ^{138}Ba has a closed neutron shell $N=82$ while the nucleus ^{134}Ba has a neutron number $N=78$, four neutrons less than the closed shell. Evaporation residues for these reaction systems were measured in the vicinity of the Coulomb barrier. The measured evaporation residue cross sections of xn and pxn channels for the reaction system ^{82}Se+^{138}Ba were considerably larger than those for the reaction system ^{82}Se+^{134}Ba, almost 100 times larger at the excitation energy (E_{ex}) region of 20–30 MeV. The fusion probabilities for these reaction systems were obtained from the evaporation residue cross sections with the aid of calculated survival probability and compared with those of the other reaction systems that make the same compound nucleus as the present systems. It was found that the fusion reaction ^{82}Se+^{138}Ba occurs without hindrance, while that of ^{82}Se+^{134}Ba is considerably hindered as commonly seen in the massive reaction system with the charge product $Z_pZ_t \geqslant 1800$ of projectile and target. The present result suggests that the neutron shell closure $N=82$ promotes fusion.

DOI: 10.1103/PhysRevC.65.054602 PACS number(s): 25.60.Pj, 24.60.Dr

I. INTRODUCTION

Fusion process between massive nuclei has been extensively investigated so far. It is well known that the fusion probability between massive nuclei depends on the charge product Z_pZ_t of projectile and target. When the charge product is less than 1800, its fusion cross section has been well reproduced by the one-dimensional barrier penetration model taking into account the coupling of inelastic excitations. On the other hand, when the charge product is larger than 1800, its fusion cross section is hindered compared with the calculated result of the model. This fact means that the interacting nuclei cannot always fuse to make a compound nucleus even if the system overcomes the entrance channel fusion barrier. In order to drive the colliding system into the formation of the compound nucleus in the heavy reaction system, where the contact point of the colliding nuclei is located outside the fission saddle point of the compound nucleus, an extra kinetic energy is needed so that the system can reach the saddle point after surmounting the fusion barrier. The necessary kinetic energy against a friction is called the extra-extra push energy (E_{xx}).

The fusion between massive nuclei depends on not only the charge product but also on the nuclear structure of the projectile and target. It is reported that the number of a valence nucleons outside a major shell affects the fusion probability [1,2]. This fact is in part correlated with the coupling of the inelastic excitations and also the nucleon transfer channels in the fusion process [1]. Recently, Oganessian *et al.* [3] measured the evaporation residue cross sections in the fusion reactions ^{130}Xe+^{86}Kr and ^{136}Xe+^{86}Kr, where the nucleus ^{136}Xe has a closed neutron shell $N=82$ and the neutron number of the nucleus ^{130}Xe is 76, six neutrons less than the closed shell. They found that the measured evaporation residue cross sections for the fusion reaction ^{136}Xe +^{86}Kr are almost two to three orders of magnitude larger than those for the fusion reaction ^{130}Xe+^{86}Kr near the Coulomb barrier region. The enhancement of the evaporation residue cross sections near the Coulomb barrier region between the double closed shell nuclei ^{208}Pb and ^{48}Ca is also pointed out in [4]. These facts suggest that the shell structure plays an important role in the low energy fusion process.

In order to investigate the effect of the nuclear shell structure on the fusion process, we investigated the isotope dependence in the fusion reactions ^{82}Se+^{134}Ba and ^{82}Se +^{138}Ba. The nucleus ^{138}Ba has a closed neutron shell $N=82$, while the nucleus ^{134}Ba has a neutron number $N=78$, four neutrons less than the $N=82$ closed shell. In the present experiments, the evaporation residue cross sections were measured as a function of excitation energy and the fusion probability was extracted from the sum of the evaporation residue cross sections with the help of a calculated survival probability. The measured fusion probabilities were compared with those in the other asymmetric or more symmetric reaction systems that make the same compound nucleus (CN) as the present reaction systems.

II. EXPERIMENTAL PROCEDURE

Evaporation residue cross sections for the fusion reactions ^{82}Se+^{138}Ba and ^{82}Se+^{134}Ba were measured by using ^{82}Se beams from the JAERI tandem booster accelerator. The targets of ^{138}Ba and ^{134}Ba were fabricated by sputtering barium carbonate on a thin aluminum foil of thickness 1.3 μm. The enrichments of the barium isotope 138 in a ^{138}Ba target and the barium isotope 134 in a ^{134}Ba target were 99.7% and 73.5%, respectively. The contaminations of the barium isotopes 135, 136, 137, and 138 in a ^{134}Ba target were 15.24%, 4.03%, 1.94%, and 5.26%, respectively. The measured thicknesses of ^{138}Ba and ^{134}Ba targets were 410 and 500 μg/cm^2, respectively. The targets were mounted on a rotating target frame and were rotated at 100 rpm during the beam irradia-

tion to prevent the targets from breaking due to the beam heating.

The details of the experimental procedure are described elsewhere [5,6]. The evaporation residues emitted in the beam direction from a target foil were separated in-flight from the primary beam by the JAERI recoil mass separator (JAERI-RMS) [7]. A carbon foil (of thickness 30 μg/cm^2) was mounted at the entrance of the JAERI-RMS to reset the charge state of the evaporation residues. The separated evaporation residues were implanted into the double-sided position-sensitive strip detector (DPSD, 73×55 mm^2) mounted at the focal position of the JAERI-RMS. The energies and the positions of incoming particles and their subsequent α-particle decays were measured by the DPSD. A clock signal was recorded at the moment of the event occurrence to construct the time interval between the implantation of the incoming particles and the successive α-decay events. The typical energy resolution was 75 keV full width at half maximum, (FWHM) for α-decay energy of 7.921 MeV from ^{216}Th produced in the present reaction.

The time-of-flight (TOF) signal of incoming particles was obtained by two microchannel-plate detectors, one mounted in front of the DPSD and the other at a distance of 30 cm upstream of the DPSD. The TOF signal was used to distinguish the incoming particles from the subsequent α-decay event. The rough estimation of the mass number of the incoming particles was obtained by a two-dimensional spectrum of the energy versus the TOF signal of the incoming particles. A silicon surface barrier detector was set at 45° with respect to the beam direction in the target chamber to measure the elastic scattering of the ^{82}Se beam from the barium target. The elastic scattering events were used to determine the absolute value of the evaporation residue cross sections.

III. DATA ANALYSIS AND EXPERIMENTAL RESULTS

All evaporation residues produced in the present fusion reactions decay by emitting α particles. Their α-decay energies and half-lives are known from the literature [8]. The identification of each evaporation residue was made event by event by measuring its subsequent α-decay energy and the time interval between the implanted evaporation residue and its decay event. In addition, the correlation of evaporation residue-α_1-α_2 chains were also used for the identification of the evaporation residue, where α_1 and α_2 are the parent and daughter α-decay events, respectively, detected at the same position in the DPSD as the implanted evaporation residue. Here a correlated event in position in the DPSD was defined by the condition $(\Delta X, \Delta Y)=(0.6$ mm, 0.6 mm) where ΔX and ΔY are the position uncertainties in the horizontal (X) and vertical (Y) directions, respectively.

The typical energy spectrum is shown in Fig. 1 for the α-decay events at the center-of-mass (c.m.) kinetic energy $E_{\mathrm{c.m.}}=225$ MeV in the fusion reaction ^{82}Se+^{138}Ba. In order to obtain the absolute evaporation residue cross sections, the transport efficiency of the evaporation residue through the JAERI-RMS was estimated by the methods given in [6,9]. The estimated transport efficiency for each evaporation residue was obtained by taking into account the charge distribution calculated by the Shima formula [10]. The typical transport efficiencies of xn, pxn, and αxn channels were 0.37, 0.31, and 0.25, respectively. Furthermore, the detection efficiency of the DPSD for full energy absorption of α particles from implanted residues, for example, ^{216}Th, was typically 0.64 at a beam energy of 323 MeV. This means that 36% of the decay events originating from the implanted residues could escape from the DPSD after depositing only a part of their kinetic energies.

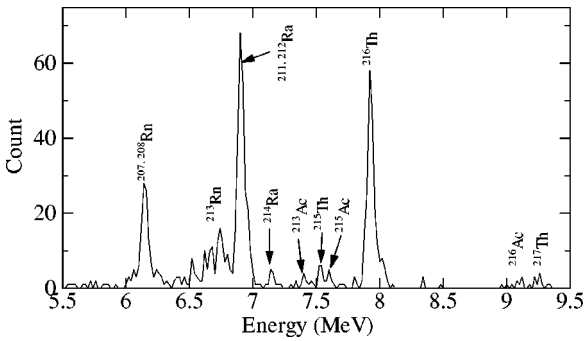

FIG. 1. Energy spectrum for the events having no TOF signal at $E_{\mathrm{c.m.}}=225$ MeV ($E_{\mathrm{ex}}=46$ MeV) for the reaction ^{82}Se+^{138}Ba.

The short-living isotopes of ^{219}Th ($T_{1/2}=1.50$ μs) and ^{218}Th ($T_{1/2}=109$ ns), which are produced in the reaction ^{82}Se+^{138}Ba, decay in part during passing through the JAERI-RMS, because the flight time in JAERI-RMS was about 1 μs. To determine the evaporation residue cross sections of ^{219}Th and ^{218}Th from the measured yields, the following assumption was made: the residues ^{219}Th and ^{218}Th decaying in flight between the position of the reset foil and the exit of the JAERI-RMS could not reach the DPSD because of the change of their charge states. Since the residue ^{218}Th has a short lifetime compared with the flight time in the JAERI-RMS, we assumed that when the residue ^{218}Th decays between the target position and the reset foil installed 16.4 cm apart from the target position, the daughter nucleus ^{214}Ra ($T_{1/2}=2.46$ s) resets its charge state after passing through the reset foil and is transported to the detector DPSD through the JAERI-RMS. We also assumed that the residue ^{219}Th decaying before reaching the exit of the JAERI-RMS is completely lost and only the surviving ^{219}Th after passing through the JAERI-RMS are detected. We neglected the small amount (0.7%) of ^{219}Th decaying between the target position and the reset foil. The angular spread of the daughter ^{214}Ra caused by the α-particle emission of ^{218}Th in-flight was simulated by assuming the isotropic emission of α particles with an energy of 9.664 MeV. This angular spread in addition to the inherent angular distribution of ^{218}Th and also the straggling due to the multiple scattering in the target was taken into account for the estimation of the transport efficiency of ^{218}Th. The transport efficiencies for ^{219}Th and ^{218}Th were thus estimated to be 0.19 and 0.04, respectively, by taking into account the charge distribution. In this case, the sum of the cross sections for the parent ^{219}Th and the daughter ^{215}Ra and also that for the parent ^{218}Th and the

TABLE I. Summary of evaporation residue cross sections for the present reactions ^{82}Se+^{138}Ba and ^{82}Se+^{134}Ba, which includes both statistical and systematical (±40%) errors.

Channel	$E_{\text{c.m.}}$ (MeV)	σ
^{82}Se+^{138}Ba		
$1n+\alpha 1n$	193	$1.8^{+1.0}_{-0.9}$ μb
	196	$8.4^{+4.6}_{-4.3}$ μb
	200	$2.6^{+1.2}_{-1.2}$ μb
	201	$6.2^{+3.2}_{-3.2}$ μb
	206	$1.0^{+0.6}_{-0.6}$ μb
	210	$0.85^{+0.55}_{-0.44}$ μb
	215	$0.44^{+0.55}_{-0.36}$ μb
	230	37^{+73}_{-37} nb
	235	70^{+90}_{-57} nb
	245	50^{+70}_{-41} nb
$2n+\alpha 2n$	193	$0.56^{+0.46}_{-0.38}$ μb
	196	$4.2^{+2.4}_{-2.3}$ μb
	200	21^{+9}_{-9} μb
	201	57^{+29}_{-29} μb
	206	$0.16^{+0.08}_{-0.08}$ mb
	210	17^{+7}_{-7} μb
	215	$3.0^{+1.5}_{-1.4}$ μb
	220	$1.6^{+0.8}_{-0.6}$ μb
	225	$0.83^{+0.47}_{-0.44}$ μb
	230	44^{+89}_{-44} nb
$3n$	201	$0.55^{+0.41}_{-0.36}$ μb
	206	21^{+11}_{-10} μb
	210	50^{+20}_{-20} μb
	215	47^{+19}_{-19} μb
	220	$5.0^{+1.5}_{-1.4}$ μb
	225	$1.7^{+1.1}_{-0.9}$ μb
	230	84^{+176}_{-84} nb
$4n$	206	$0.19^{+0.20}_{-0.15}$ μb
	210	$1.2^{+0.6}_{-0.6}$ μb
	215	17^{+7}_{-7} μb
	220	21^{+5}_{-5} μb
	225	14^{+7}_{-7} μb
	230	$3.8^{+1.6}_{-1.6}$ μb
	235	$0.62^{+0.32}_{-0.29}$ μb
	240	$0.15^{+0.12}_{-0.09}$ μb
	245	23^{+48}_{-23} nb
$5n$	220	$0.54^{+0.46}_{-0.32}$ μb
	225	$1.3^{+0.8}_{-0.7}$ μb
	230	$3.6^{+1.5}_{-1.5}$ μb
	235	$4.1^{+1.8}_{-1.7}$ μb
	240	$1.3^{+0.6}_{-0.6}$ μb
	245	$0.42^{+0.23}_{-0.21}$ μb
	251	$0.21^{+0.14}_{-0.12}$ μb
$6n+7n$	230	$0.16^{+0.15}_{-0.11}$ μb
	235	$0.42^{+0.27}_{-0.22}$ μb
	240	$1.1^{+0.6}_{-0.5}$ μb
	245	$1.1^{+0.4}_{-0.4}$ μb
	251	$0.87^{+0.43}_{-0.38}$ μb
$p3n$	220	$1.2^{+0.7}_{-0.49}$ μb
	225	$3.4^{+2.2}_{-1.9}$ μb
	230	$2.6^{+1.3}_{-1.3}$ μb
	235	$0.70^{+0.40}_{-0.34}$ μb
	240	$0.12^{+0.12}_{-0.09}$ μb
$p4n$	220	$0.41^{+0.79}_{-0.41}$ μb
	225	$0.32^{+0.40}_{-0.26}$ μb
	230	$4.7^{+2.0}_{-2.0}$ μb
	235	$4.7^{+2.0}_{-1.9}$ μb
	240	$4.1^{+1.7}_{-1.7}$ μb
	245	$2.4^{+0.9}_{-0.9}$ μb
	251	$0.52^{+0.27}_{-0.26}$ μb
$p5n$	230	$0.42^{+0.32}_{-0.25}$ μb
	235	$1.2^{+0.8}_{-0.6}$ μb
	240	$5.7^{+2.5}_{-2.4}$ μb
	245	$8.5^{+3.5}_{-3.5}$ μb
	251	$8.4^{+3.6}_{-3.4}$ μb
$p6n+p7n$	240	$0.20^{+0.17}_{-0.13}$ μb
	245	$0.53^{+0.27}_{-0.25}$ μb
	251	$2.0^{+0.8}_{-0.8}$ μb
$\alpha 4n+\alpha 5n$	230	$6.9^{+6.2}_{-6.1}$ μb
	235	22^{+11}_{-11} μb
	240	25^{+11}_{-11} μb
	245	18^{+7}_{-7} μb
	251	10^{+4}_{-4} μb
$\alpha 6n+\alpha 7n$	245	$2.7^{+1.6}_{-1.6}$ μb
	251	$3.5^{+1.8}_{-1.8}$ μb
^{82}Se+^{134}Ba		
$1n$	200	62^{+78}_{-51} nb
	204	$0.19^{+0.14}_{-0.12}$ μb
	209	$0.26^{+0.17}_{-0.14}$ μb
	214	$0.48^{+0.31}_{-0.27}$ μb
	221	$0.41^{+0.35}_{-0.26}$ μb
	232	62^{+128}_{-62} nb
	235	73^{+147}_{-73} nb
	239	51^{+59}_{-32} nb
	245	38^{+82}_{-38} nb
$2n+3n$	200	86^{+54}_{-48} nb
	204	$0.39^{+0.17}_{-0.17}$ μb
	209	$0.88^{+0.32}_{-0.32}$ μb
	214	$0.79^{+0.34}_{-0.34}$ μb
	221	$0.11^{+0.10}_{-0.07}$ μb

TABLE I. (*Continued*).

Channel	$E_{\mathrm{c.m.}}$ (MeV)	σ	Channel	$E_{\mathrm{c.m.}}$ (MeV)	σ
	232	81^{+99}_{-66} nb		235	$0.78^{+0.42}_{-0.40}$ μb
	235	$0.14^{+0.15}_{-0.10}$ μb		239	$0.57^{+0.19}_{-0.18}$ μb
	239	96^{+54}_{-42} nb		240	$0.56^{+0.32}_{-0.28}$ μb
	240	$0.11^{+0.11}_{-0.08}$ μb		245	$0.40^{+0.23}_{-0.20}$ μb
	245	51^{+69}_{-41} nb		249	$0.29^{+0.17}_{-0.15}$ μb
$4n+5n$	221	84^{+86}_{-59} nb	$p4n+p5n$	232	$0.56^{+0.29}_{-0.27}$ μb
	232	45^{+95}_{-45} nb		235	$0.36^{+0.27}_{-0.27}$ μb
	235	48^{+102}_{-48} nb		239	$0.13^{+0.07}_{-0.05}$ μb
	249	19^{+38}_{-19} nb		240	$0.31^{+0.22}_{-0.17}$ μb
				245	$0.26^{+0.17}_{-0.14}$ μb
p	204	$9.5^{+19.5}_{-9.5}$ nb		249	$0.11^{+0.10}_{-0.07}$ μb
	209	28^{+30}_{-20} nb	$\alpha+\alpha 1n$	232	$2.0^{+1.0}_{-0.9}$ μb
	214	61^{+129}_{-61} nb		235	$0.60^{+0.40}_{-0.36}$ μb
	221	$0.28^{+0.16}_{-0.14}$ μb		239	$1.4^{+0.6}_{-0.6}$ μb
	232	$0.20^{+0.15}_{-0.12}$ μb		240	$0.87^{+0.43}_{-0.41}$ μb
	235	$0.17^{+0.22}_{-0.14}$ μb		245	$0.82^{+0.36}_{-0.36}$ μb
	239	89^{+51}_{-39} nb		249	$0.34^{+0.17}_{-0.16}$ μb
	240	$0.19^{+0.19}_{-0.13}$ μb			
$5n+p1n+\alpha 5n$	204	$0.28^{+0.15}_{-0.13}$ μb	$\alpha 2n+\alpha 3n$	214	$0.90^{+0.80}_{-0.77}$ μb
	209	$0.30^{+0.15}_{-0.14}$ μb		221	$1.7^{+0.8}_{-0.7}$ μb
	214	$0.77^{+0.35}_{-0.35}$ μb		232	$1.6^{+0.7}_{-0.7}$ μb
	221	$0.41^{+0.27}_{-0.23}$ μb		235	$1.0^{+0.6}_{-0.5}$ μb
	232	$0.77^{+0.43}_{-0.40}$ μb		239	$1.0^{+0.5}_{-0.5}$ μb
	235	$0.37^{+0.31}_{-0.24}$ μb		240	$0.70^{+0.40}_{-0.36}$ μb
	239	$0.48^{+0.19}_{-0.17}$ μb		245	$0.80^{+0.40}_{-0.37}$ μb
	240	$0.37^{+0.28}_{-0.22}$ μb		249	$0.79^{+0.32}_{-0.32}$ μb
	245	$0.31^{+0.22}_{-0.18}$ μb			
	249	$0.26^{+0.17}_{-0.14}$ μb	$\alpha 4n+\alpha 5n$	232	$0.28^{+0.27}_{-0.17}$ μb
				235	$0.32^{+0.28}_{-0.21}$ μb
$p2n+p3n$	204	16^{+32}_{-16} nb		239	$0.62^{+0.31}_{-0.29}$ μb
	209	$0.36^{+0.16}_{-0.16}$ μb		240	$0.19^{+0.20}_{-0.13}$ μb
	214	$1.2^{+0.5}_{-0.5}$ μb		245	46^{+93}_{-46} nb
	221	$1.6^{+0.7}_{-0.7}$ μb		249	$0.19^{+0.14}_{-0.11}$ μb
	232	$1.1^{+0.5}_{-0.5}$ μb			

daughter ^{214}Ra were obtained using the yields of the products ^{215}Ra and ^{214}Ra, respectively.

We assumed that the nucleus ^{215}Ra measured in the energy regions $E_{\mathrm{cm}} \leqslant 201$ MeV, 206 MeV$\leqslant E_{\mathrm{cm}} \leqslant 215$ MeV, and $E_{\mathrm{cm}} \geqslant 230$ MeV is produced by the $1n$ channel, the αn channel, and the $2p3n$ channel, respectively. We also assumed that the nucleus ^{214}Ra measured in the energy regions $E_{\mathrm{cm}} \leqslant 206$ MeV and $E_{\mathrm{cm}} \geqslant 215$ MeV is produced by the $2n$ channel and the $\alpha 2n$ channel, respectively. Since the ^{214}Ra data measured at the energy $E_{\mathrm{cm}} = 210$ MeV corresponds to the middle of the overlapping region of these two components, we assumed that half of the yields is produced by the $2n$ channel and the rest half of the yields is produces by the $\alpha 2n$ channel.

The obtained evaporation residue cross sections for the present reactions are listed in Table I, and are also shown in Figs. 2 and 3 as a function of c.m. energy determined in the middle of the target layer together with the calculated results using the HIVAP code [11]. The details of these calculations will be shown in the following section. The experimental error for the data includes both statistical and systematical contribution, where the systematical uncertainty was estimated to be 40% by taking into account the uncertainties from the transport efficiency and the charge distribution of evaporation residue.

IV. DISCUSSIONS

The measured evaporation residue cross sections were compared with theoretical calculations. In the present theo-

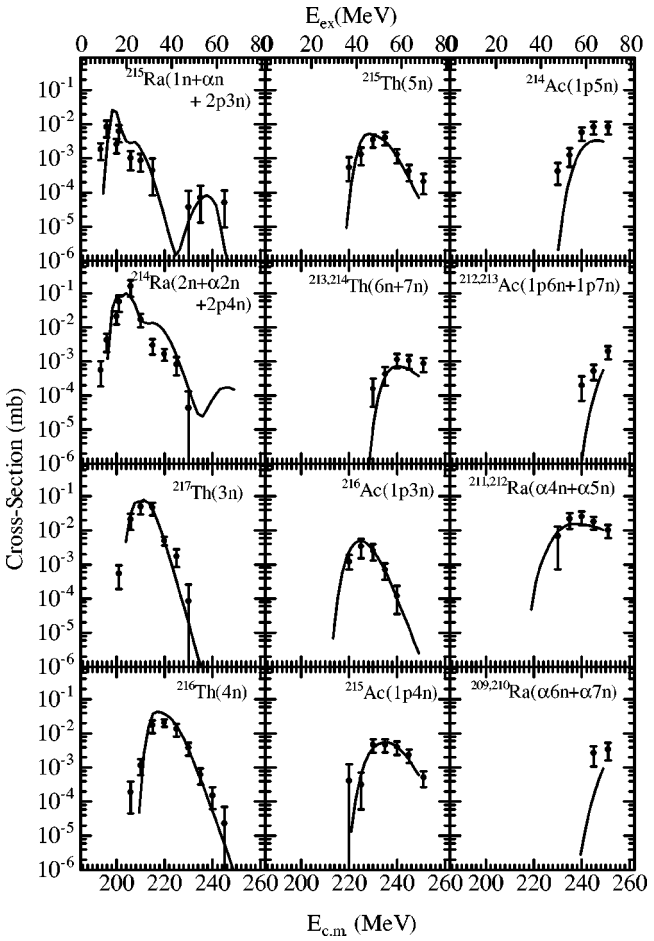

FIG. 2. Evaporation residue cross sections for the reaction ^{82}Se+^{138}Ba with the calculated ones that were estimated by using the statistical model code HIVAP. In the calculation of the fusion cross section, the coupling of inelastic excitations of the first 2^+ and 3^- states for both the target and projectile to the fusion process were taken into account by the use of the code CCDEF. Error bars represent not only the statistical contribution but also the systematical one of 40%.

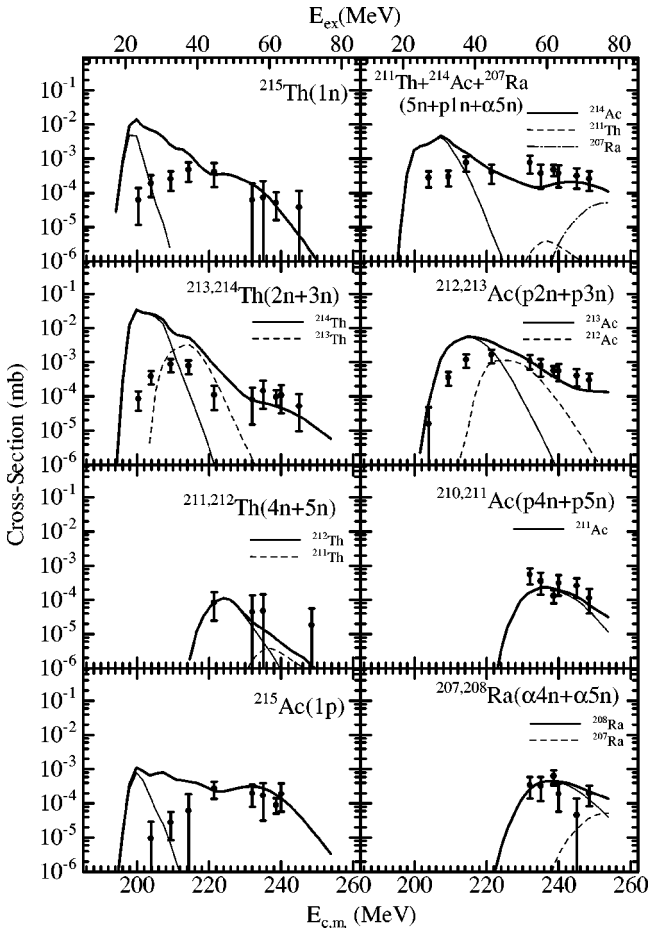

FIG. 3. Same as Fig. 2 except for the reaction ^{82}Se+^{134}Ba. The thick curve in each channel is the calculated result including the components originating from the fusion reactions ^{82}Se+^{A}Ba, where $A \geqslant 135$. The percentage of the heavier barium isotopes 135, 136, 137, and 138 in a ^{134}Ba target were 15.24%, 4.03%, 1.94%, and 5.26%, respectively. The thin curve shows the component originating from the fusion reaction ^{82}Se+^{134}Ba.

retical calculation, first, the fusion cross section was estimated by the coupled-channel calculation using the code CCDEF [12]. After that, the survival probability of each evaporation residue was calculated by using the statistical model code HIVAP. In the calculation of the fusion cross section, the coupling of the inelastic excitations of the first 2^+ and 3^- states for both the projectile and the target to the fusion process were taken into account. The adopted deformation parameters of the first quadruple and octupole vibrations were $\beta_2=0.164$ [13] and $\beta_3=0.124$ [14] for ^{134}Ba and $\beta_2=0.093$ [13] and $\beta_3=0.118$ [14] for ^{138}Ba. These for the projectile ^{82}Se were $\beta_2=0.194$ [13] and $\beta_3=0.161$ [14]. The calculated fusion cross sections for both reaction systems show enhancement below their Bass barriers ($V_{\rm Bass}=207.8$ MeV for the fusion reaction of ^{82}Se+^{134}Ba and 206.6 MeV for the fusion reaction of ^{82}Se+^{138}Ba), where the calculated barriers were shifted toward lower energy by about 10 MeV compared with the calculation without taking into account the coupling of these inelastic excitations. The calculated barrier shifts are almost the same as in the present reaction systems except for a small difference of about 1 MeV.

In the statistical model calculation, there are several important parameters such as level density parameters at the equilibrium deformation and the saddle point deformation, the binding energies of emitted neutrons, protons, and α particles, and the fission barrier. We used the formula of [15] to calculate the level density parameters. Here the shell damping effect as a function of the excitation energy ($E_{\rm ex}$) was taken into account as proposed by Ignatyuk *et al.* [16]. The shell damping parameter of 18 MeV was assumed. We also took into account the collective (rotational and vibrational) enhancement of the level density as pointed out by Junghans *et al.* [17]. The rotational enhancement factor $K_{\rm rot}(E_{\rm ex})$ was calculated according to the procedure of [17] and the vibrational enhancement factor $K_{\rm vib}(E_{\rm ex})$ was calculated using the formula of [18]. The critical deformation parameter β_2 to distinguish a deformed nucleus from a spherical nucleus was assumed to be 0.17 in the estimation of the level density. The

calculated β_2 value of [19] for ground state deformation was used for nuclei encountered in the deexitation process of the compound nucleus. As for the ground state mass, we used the mass table of Audi and Wapstra [20]. The fission barrier B_f was calculated as $B_f = aB_{LD} - E_s$, where B_{LD} is the liquid drop fission barrier of [21] and E_s is the shell correction energy. The scaling parameter a was fixed to be 1. The shell correction energy was estimated to be the difference of the experimental mass [20] and the calculated liquid drop mass [22].

As seen in Fig. 2, the maximum evaporation residue cross sections of the $2n$ and $3n$ channels in the reaction ^{82}Se $+ ^{138}$Ba are about 100 μb and are quite consistent with the calculated evaporation residue cross sections for these channels. The calculated evaporation residue cross sections of the $1n$ channel is limited at the low energy side by the fusion barrier. The measured cross section of the $1n$ channel also shows such an effect because the peak position of the $1n$ channel cross section is shifted to an excitation energy of 18 MeV. It is noted that the evaporation residue cross sections measured below the Bass barrier V_{Bass} are well reproduced by the present calculation, indicating the significance of the coupling of the inelastic excitations of the 2^+ and 3^- states.

The excellent agreement between the measured evaporation residue cross sections and the calculated results means that the fusion in the reaction ^{82}Se$+ ^{138}$Ba is properly simulated by the CCDEF calculation without any fusion hindrance. This is not true for the so-called extra push systematics of Quint *et al.* [1], where measured extra-extra push energies E_{xx} are plotted as a function of the charge product Z_pZ_t of the projectile and target plus a nuclear shell correction $10\nu_{min}$. The small factor ν_{min} is defined as $\nu_{min} = \min(\Delta Z_p, \Delta N_p) + \min(\Delta Z_t, \Delta N_t)$, where $\Delta Z_{p,t}$ and $\Delta N_{p,t}$ are the numbers of valence particles or holes from the nearest major closed shell of projectile (p) and target (t). From this systematics we expect an extra-extra push energy around 10–15 MeV for the present reaction ^{82}Se$+ ^{138}$Ba. This effectively makes the fusion barrier high and considerably decreases the $1n$ and $2n$ channels cross sections at the low excitation energy region $E_{ex} \leqslant 30$ MeV. There is no such evidence seen in the excitation function shown in Fig. 2.

On the other hand, the measured evaporation residue cross sections in the fusion reaction ^{82}Se$+ ^{134}$Ba show clear deviations from the calculated cross sections mainly in the low excitation energy region $E_{ex} = 20-30$ MeV as shown in Fig. 3. Since the present target of ^{134}Ba has the admixture of the other isotopes of barium, we can see a sizable contribution of the fusion products originating from the fusion reactions ^{82}Se$+ ^{A}$Ba, where $A \geqslant 135$. However, these contributions mainly concentrate on excitation energies higher than 40 MeV except for the residues ^{211,212}Th, ^{210,211}Ac, and ^{207,208}Ra. According to the present calculation, these residues are produced only by the fusion ^{82}Se$+ ^{134}$Ba in the energy region ($50 \leqslant E_{ex} \leqslant 70$ MeV). Large deficits of the evaporation residue cross sections are seen, for instance, in the $1n$ (^{215}Th), $2n+3n$ (^{213,214}Th), and also the $1p$ (^{215}Ac) channels at $E_{ex} = 20-30$ MeV, where the main contribution is ascribed to the fusion ^{82}Se$+ ^{134}$Ba. The observed cross sections corresponding to the maximum of the $2n+3n$ channels are 0.1–0.5 μb, which are more than two orders of magnitude too small compared with the maximum cross section of the $2n$ or $3n$ channel in the fusion ^{82}Se$+ ^{138}$Ba.

It is important to verify the survival probability calculated in the HIVAP code by using the experimental Γ_n/Γ_f value of [23]. Here the decay widths of the neutron and fission are denoted by Γ_n and Γ_f, respectively. Schmidt *et al.* obtained average Γ_n/Γ_f values from the $4n$ channel evaporation residue cross sections for the compound nucleus ^{A}Th ($214 \leqslant A \leqslant 220$). We can estimate the Γ_n/Γ_f values for the compound nuclei ^{216}Th and ^{220}Th as 0.07 and 0.18, respectively. Then the ratio P of the Γ_n/Γ_f value for ^{216}Th to ^{220}Th is $P \approx 0.4$. Since the dependence of the Γ_n/Γ_f values on the excitation energy is similar to each other for the compound nuclei ^{216}Th and ^{220}Th, the ratio P depends weakly on the excitation energy. The present calculation shows $P = 0.3 \sim 0.5$ at $20 \leqslant E_{ex} \leqslant 80$ MeV. Using this experimental value, we can roughly estimate $\sigma_{1n}(^{216}\text{Th}) \approx P\sigma_{1n}(^{220}\text{Th})$ and $\sigma_{2n}(^{216}\text{Th}) \approx P^2\sigma_{2n}(^{220}\text{Th})$, where the $1n$ and $2n$ channel cross sections originating from the CN are denoted by σ_{1n}(CN) and σ_{2n}(CN), respectively. This simple consideration shows that $\sigma_{1n}(^{216}\text{Th}) \approx 0.4\sigma_{1n}(^{220}\text{Th})$ and $\sigma_{2n}(^{216}\text{Th}) \approx 0.15\sigma_{2n}(^{220}\text{Th})$. The fact that the $1n$ and $2n$ channel cross sections for the compound nucleus ^{216}Th are smaller than the compound nucleus ^{220}Th is mainly due to the increasing neutron binding energy with decreasing mass number of the thorium isotope. These estimations are consistent with the HIVAP calculation shown in Figs. 2 and 3. Contrary to the estimation, the measured $1n$ and $2n$ channel cross sections for the fusion reaction ^{82}Se$+ ^{134}$Ba are smaller by two orders of magnitude than those for the fusion reaction of ^{82}Se$+ ^{138}$Ba. We also checked the contribution of the shell energy to the fission barrier in the present calculation, because both the excited compound nuclei and also the excited daughter nuclei are close to the $N = 126$ shell. If the shell damping parameter is decreased from 18 MeV to a few MeV, the calculated $1n$ and $2n+3n$ channel cross sections for ^{82}Se$+ ^{134}$Ba decrease to the experimental values at $E_{ex} \approx 20-30$ MeV. But, at the same time, the calculated $2n$ and also $3n$ channel cross-sections for ^{82}Se$+ ^{138}$Ba also decrease by two orders of magnitude. This means that the strong shell energy around $N = 126$ is not the cause of the observed deficit in ^{82}Se $+ ^{134}$Ba. Thus this deficit cannot be ascribed to the evaporation process in the fusion reaction ^{82}Se$+ ^{134}$Ba, but can rather be ascribed to the fusion process.

From the measured evaporation residue cross sections we can extract the fusion probability with the aid of calculated survival probability as follows:

$$\langle P_{fus}(E_{c.m.}) \rangle = \frac{\sum_c \sigma_{er,c}(E_{c.m.})}{\pi \lambda^2 \sum_l (2l+1) \sum_c w_{er,c}(E_{ex}, l)}, \quad (1)$$

where the fusion probability $\langle P_{fus} \rangle$ is an averaged value weighted by the angular momentum l. Actually, in the

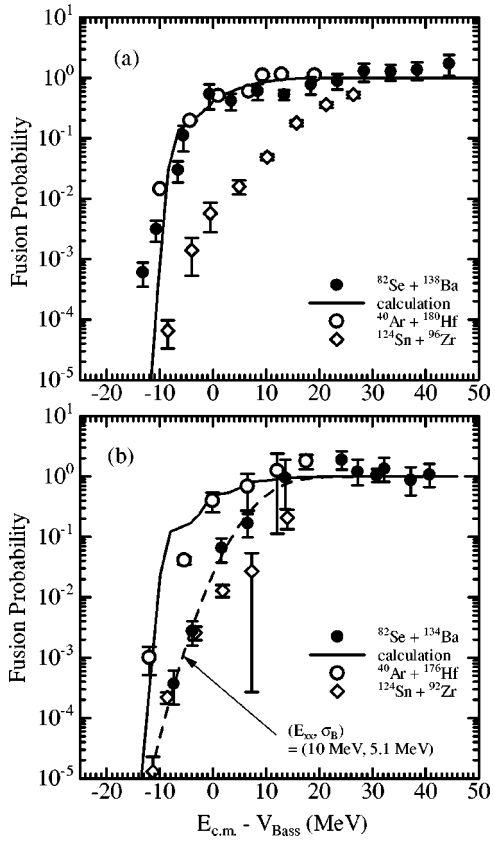

FIG. 4. Fusion probabilities obtained from the measured evaporation residue cross sections for the reactions (a) ^{82}Se+^{138}Ba and (b) ^{82}Se+^{134}Ba as a function of $E_{\mathrm{c.m.}}-V_{\mathrm{Bass}}$ (MeV), where V_{Bass} is the Bass fusion barrier. The solid curve shows the fusion probability with no fusion hindrance calculated by the code CCDEF, which includes the coupling of inelastic excitations of the first 2^+ and 3^- states. The dashed curve of (b) is the fusion probability calculated by the expression in [1,25] assuming $(E_{\mathrm{xx}},\ \sigma_{\mathrm{B}})=(10$ MeV, 5.1 MeV) (see text). The data for ^{40}Ar+^{176,180}Hf [24] and ^{124}Sn +^{92,96}Zr [25] are also plotted to make a comparison with the present data.

present reactions, the angular momentum contributions to the evaporation residue production is from $0\hbar$ to $20\hbar$, because of a large fission probability for a large l value. Therefore the obtained fusion probability is considered to be that for the central collision. The survival probability $w_{\mathrm{er,c}}$ as a function of the excitation energy $E_{\mathrm{ex}}\equiv E_{\mathrm{c.m.}}+Q$ (reaction Q value) for a specific channel c and angular momentum l was calculated by using HIVAP. The fusion probability for the reaction ^{82}Se+^{134}Ba was obtained by subtracting the other contribution ascribed to the heavier barium isotopes than ^{134}Ba. Especially the cross sections of ^{213,214}Th at $E_{\mathrm{ex}}=24$ and 27 MeV, ^{212,213}Ac at $E_{\mathrm{ex}}=33$ and 38 MeV, and also those of ^{211,212}Th and ^{210,211}Ac at $E_{\mathrm{ex}}\geqslant 45$ MeV were used, because there is a negligible contribution to these residues from the fusion products in the reaction ^{82}Se+^{A}Ba ($A\geqslant 135$) based on the present statistical model calculation.

The results are shown in Fig. 4 as a function of $E_{\mathrm{c.m.}}-V_{\mathrm{Bass}}$ together with the calculated ones (solid curve). They are also compared with those of the asymmetric reactions ^{40}Ar+^{176,180}Hf ($Z_pZ_t=1296$) [24] and the more symmetric reactions ^{124}Sn+^{92,96}Zr ($Z_pZ_t=2000$) [25], where the same compound nuclei ^{216}Th and ^{220}Th as in the present work are produced. As shown in Fig. 4, the fusion probability for the reaction ^{82}Se+^{138}Ba is very close to that of ^{40}Ar+^{180}Hf and consistent with the calculation, while it is clearly different from that of ^{124}Sn+^{96}Zr. On the other hand, the fusion probability for the reaction ^{82}Se+^{134}Ba deviates from that of ^{40}Ar+^{176}Hf and also from the calculation. It is rather close to the ^{124}Sn+^{92}Zr case below the Bass barrier. The present results indicate that there is no fusion hindrance for the reaction ^{82}Se+^{138}Ba, while for the reaction ^{82}Se+^{134}Ba the fusion around the Coulomb barrier is hindered.

In order to obtain the extra-extra push energy for the reaction ^{82}Se+^{134}Ba, we used the expression proposed in [1,25], where a fusion barrier distribution of a Gaussian shape having the mean value E_{B} and variance σ_{B}^2 was assumed. In this analysis, the transmission coefficient of the Hill-Wheeler type [26] with $\hbar\omega=3.0$ MeV was used and we ignored the contribution of the centrifugal potential to the fusion potential, because the centrifugal potential is very small (only 0.8 MeV at $l=20\hbar$) in the present reaction systems. From this analysis we obtained the extra-extra push parameters $(E_{\mathrm{xx}},\sigma_{\mathrm{B}})=(10$ MeV, 5.1 MeV) for the reaction ^{82}Se+^{134}Ba. These values are quite consistent with the systematics of [1].

The present result suggests that the fusion process after surmounting the fusion barrier may be different in the reactions ^{82}Se+^{138}Ba and ^{82}Se+^{134}Ba. The target nucleus ^{138}Ba has the closed neutron shell $N=82$ and the target nucleus ^{134}Ba has the neutron number $N=76$, only four neutrons less than the closed shell. The projectile nucleus ^{82}Se is also close to the closed neutron shell $N=50$. The calculated subbarrier fusion enhancement due to the coupling of the inelastic excitations of 2^+ and 3^- states is almost the same in both the present reactions mentioned above, because the deformation parameters β_2 and β_3 are similar to each other for both the isotopes ^{134}Ba and ^{138}Ba. In the present calculation, the coupling to the neutron transfer channel was not included. The effect of the neutron transfer during the sub-barrier fusion process can be roughly estimated by the Q values for the pickup and the strip reactions. The Q values for one- and two-neutron transfers are negative for the reaction ^{82}Se +^{138}Ba, while the Q value for the two-neutron transfer is positive, 0.79 MeV, for the strip reaction of ^{82}Se+^{134}Ba. This may result in the more sub-barrier enhancement in the fusion reaction ^{82}Se+^{134}Ba than the case of ^{82}Se+^{138}Ba. This expectation is in contradiction with the present experimental results.

The importance of the shell energy in the fusion process is pointed out by Myers and Swiatecki [27]. They suggest that the shell energy resists neck growth at the time of contact between the projectile and target, and then the projectile nucleus can go deeply into the target nucleus with a small kinetic energy dissipation. This process is also suggested by the theoretical calculation of Möller *et al.* [28], where the single particle levels for the two-center system of closed shell nuclei show a prominent energy gap up to a short

distance between mass centers. This qualitatively suggests a small friction during the fusion process of closed shell nuclei.

Oganessian suggests the important relation between the fusion process and the fission process [29]. The compound nucleus ^{220}Th at low excitation energy can decay into asymmetric fission fragments, where the heavy fragment is concentrated around the atomic number $Z=54$ with a narrow charge width 4.7 (FWHM) [30]. The compound nucleus ^{216}Th has no such asymmetric fission component. The target and projectile combination for the fusion reaction ^{82}Se $+^{138}$Ba is close to the asymmetric fission components of ^{220}Th. Also in the case of the fusion reaction ^{136}Xe$+^{86}$Kr, the compound nucleus ^{222}Th has asymmetric fission fragments close to ^{86}Kr and ^{136}Xe. Both the fusion reactions (^{82}Se$+^{138}$Ba and ^{136}Xe$+^{86}$Kr) show large evaporation residue cross sections in the present work and in [3]. In these cases, the two asymmetric fission fragments are spherical and thus have a compact shape at scission. Such a combination of the target and projectile may follow the fission valley in the reverse way to reach the fission saddle point.

V. CONCLUSION

Evaporation residues from the reactions ^{82}Se$+^{138}$Ba and ^{82}Se$+^{134}$Ba were measured to investigate the dependence of the fusion reaction on the nuclear shell structure of the colliding nuclei. The nucleus ^{138}Ba has the closed neutron shell $N=82$ while the nucleus ^{134}Ba has a neutron number $N=78$, four neutrons less than the closed shell. The measured evaporation residue cross sections for the reaction ^{82}Se $+^{138}$Ba were almost two orders of magnitude larger near the Coulomb barrier region than those for the reaction ^{82}Se $+^{134}$Ba. This large difference is ascribed to the entrance channel of the fusion process. The fusion probabilities obtained from the measured evaporation residue cross sections with the aid of the calculated survival probability were compared with the other reaction systems, that is, the asymmetric systems ^{40}Ar$+^{180,176}$Hf and also the more symmetric systems ^{124}Sn$+^{96,92}$Zr. These make the same compound nuclei as the present systems. From these comparisons, we conclude that there is no fusion hindrance for the reaction system ^{82}Se$+^{138}$Ba, while the fusion for the reaction system ^{82}Se$+^{134}$Ba is considerably hindered near the Coulomb barrier. The obtained extra-extra push parameters $(E_{xx},\sigma_B)=(10\ \text{MeV},5.1\ \text{MeV})$ for the reaction ^{82}Se$+^{134}$Ba were consistent with the systematics of Quint *et al.* [1] of the extra-extra push phenomena.

The present result suggests that the fusion of massive reaction systems strongly depends on the shell structure of colliding partners. It is important to realize theoretically the energy dissipation due to the friction after contact by taking into account the shell structure of colliding nuclei. Further experimental investigation is needed to confirm the importance of the shell closure in the fusion process, and also make the relation between fusion and fission clear.

ACKNOWLEDGMENT

The authors thank the crew of the JAERI tandem-booster facility for the beam operation.

[1] A. B. Quint, W. Reisdorf, K.-H. Schmidt, P. Armbruster, F. P. Hessberger, S. Hofmann, J. Keller, G. Münzenberg, H. Stelzer, H.-G. Clerc, W. Morawek, and C.-C. Sahm, Z. Phys. A **346**, 119 (1993).

[2] K.-H. Schmidt and W. Morawek, Rep. Prog. Phys. **54**, 949 (1991).

[3] Yu. Ts. Oganessian, A. Yu. Lavrentev, A. G. Popeko, R. N. Sagaidak, A. V. Yeremin, S. H. Hofmann, F. P. Hessberger, V. Ninov, and C. Stodel, JINR, Scientific Report 1995-1996, 1997 (unpublished).

[4] Yu. Ts. Oganessian, V. K. Utyonkov, Yu. V. Lobanov, F. S. Abdullin, A. N. Polyakov, I. V. Shirokovsky, Yu. S. Tsyganov, A. N. Mezentsev, S. Iliev, V. G. Subbotin, A. M. Sukhov, K. Subotic, O. V. Ivanov, A. N. Voinov, V. I. Zagrebaev, K. J. Moody, J. F. Wild, N. J. Stoyer, M. A. Stoyer, and R. W. Lougheed, Phys. Rev. C **64**, 054606 (2001).

[5] S. Mitsuoka, H. Ikezoe, K. Nishio, and J. Lu, Phys. Rev. C **62**, 054603 (2000).

[6] K. Nishio, H. Ikezoe, S. Mitsuoka, and J. Lu, Phys. Rev. C **62**, 014602 (2000); K. Nishio, H. Ikezoe, S. Mitsuoka, K. Satou, and S. C. Jeong, *ibid.* **63**, 044610 (2001).

[7] H. Ikezoe, Y. Nagame, T. Ikuta, S. Hamada, I. Nishinaka, and T. Ohtuki, Nucl. Instrum. Methods Phys. Res. A **376**, 420 (1996).

[8] R. B. Firestone, in *Table of Isotopes*, edited by V. S. Shirley (Wiley, New York, 1996).

[9] T. Kuzumaki, H. Ikezoe, S. Mitsuoka, T. Ikuta, S. Hamada, Y. Nagame, I. Nishinaka, and O. Hashimoto, Nucl. Instrum. Methods Phys. Res. A **437**, 107 (1999).

[10] K. Shima, T. Ishihara, and T. Mikuno, Nucl. Instrum. Methods Phys. Res. **200**, 605 (1982).

[11] W. Reisdorf and M. Schädel, Z. Phys. A **343**, 47 (1992).

[12] J. O. Fernández Niello, C. H. Dasso, and S. Landowne, Comput. Phys. Commun. **54**, 409 (1989).

[13] S. Raman, C. H. Malarkey, W. T. Milner, C. W. Nestor, Jr., and P. H. Stelson, At. Data Nucl. Data Tables **36**, 1 (1987).

[14] R. H. Spear, At. Data Nucl. Data Tables **42**, 55 (1989).

[15] W. Reisdorf, Z. Phys. A **300**, 227 (1981).

[16] A. V. Ignatyuk, G. N. Smirenkin, and A. S. Tishin, Sov. J. Nucl. Phys. **21**, 255 (1975).

[17] A. R. Junghans, M. de Jong, H.-G. Clerc, A. V. Ignatyuk, G. A. Kudyaev, and K.-H. Schmidt, Nucl. Phys. **A629**, 635 (1998).

[18] A. S. Iljinov, M. V. Medel, N. Bianchi, E. de Sanctis, C. Guaraldo, V. Luchierini, V. Muccifora, E. Polli, A. R. Reolon, and P. Rossi, Nucl. Phys. **A543**, 517 (1992).

[19] P. Möller, J. R. Nix, W. D. Myers, and W. J. Swiatecki, At. Data Nucl. Data Tables **59**, 185 (1995).

[20] G. Audi and A. H. Wapstra, Nucl. Phys. **A595**, 409 (1995).

[21] S. Cohen, F. Plasil, and W. J. Swiatecki, Ann. Phys. (N.Y.) **82**, 557 (1974).
[22] W. D. Myers and W. J. Swiatecki, Ark. Fys. **36**, 343 (1967).
[23] K.-H. Schmidt, W. Faust, G. Münzenberg, W. Reisdorf, H.-G. Clerc, D. Vermeulen, and W. Lang, *International Symposium on Physics and Chemistry of Fission* (IAEA, Vienna, 1979), Vol. 1, p. 409.
[24] H.-G. Clerc, J. G. Keller, C.-C. Sahm, K.-H. Schmidt, H. Schulte, and D. Vermeulen, Nucl. Phys. **A419**, 571 (1984).
[25] C.-C. Sahm, H.-G. Clerc, K.-H. Schmidt, W. Reisdorf, P. Armbruster, F. P. Hessberger, J. G. Keller, G. Münzenberg, and D. Vermeulen, Nucl. Phys. **A441**, 316 (1985).
[26] D. L. Hill and J. A. Wheeler, Phys. Rev. **89**, 1102 (1953).
[27] W. D. Myers and W. J. Swiatecki, Phys. Rev. C **62**, 044610 (2000).
[28] P. Möller, R. Nix, P. Armbruster, S. Hofmann, and G. Münzenberg, Z. Phys. A **359**, 251 (1997).
[29] Yu. Ts. Oganessian, in *Heavy Elements and Related New Phenomena*, edited by W. Greiner and R. K. Gupta (World Scientific, Singapore, 1999), Vol. 1, p. 43.
[30] K.-H. Schmidt, S. Steinhäuser, C. Böckstiegel, A. Grewe, A. Heinz, A. R. Junghans, J. Benlliure, H.-G. Clerc, M. de Jong, J. Müller, M. Pfützner, and B. Voss, Nucl. Phys. **A665**, 221 (2000).